Chinese Chemical Letters 31 (2020) 547–550

Contents lists available at ScienceDirect

Chinese Chemical Letters

journal homepage: www.elsevier.com/locate/cclet

Communication

All-solid-state $BiVO_4/ZnIn_2S_4$ Z-scheme composite with efficient charge separations for improved visible light photocatalytic organics degradation

Deling Yuan, Mengting Sun, Shoufeng Tang*, Yating Zhang, Zetao Wang, Jinbang Qi, Yandi Rao, Qingrui Zhang

Hebei Key Laboratory of Heavy Metal Deep-Remediation in Water and Resource Reuse, School of Environmental and Chemical Engineering, Yanshan University, Qinhuangdao 066004, China

ARTICLE INFO

Article history:
Received 24 August 2019
Received in revised form 19 September 2019
Accepted 27 September 2019
Available online 30 September 2019

Keywords:
Z-scheme composite
$BiVO_4$
$ZnIn_2S_4$
Visible light photocatalysis
Charge separation
Organic pollutant degradation

ABSTRACT

Constructing a Z-scheme is a significant approach to improve the separation of photogenerated carriers for effective organic pollutant degradation. Herein, a $BiVO_4/ZnIn_2S_4$ (BZ) Z-scheme composite was successfully synthesized, and applied to photodegrade methyl orange (MO) irradiated by a LED lamp. Anchoring the $BiVO_4$ on the $ZnIn_2S_4$ nanoparticles promoted the separation of photogenerated electron-holes and broadened the light response range. The detailed characterizations, including surface morphology, elements valence state, and photocurrent performance, demonstrated that the enhanced separation of photogenerated carriers was the pivotal reason for the enhanced photocatalysis reaction. Benefiting from the excellent photocatalytic characteristics, the 5% mass ratio of BZ composite presented the highest MO degradation rate of 0.00997 min^{-1}, which was 1.9 and 10.3 times greater than the virgin $ZnIn_2S_4$ and $BiVO_4$, respectively. Furthermore, the BZ hybrid materials indicated a well photo-stability in the four recycling tests.

Although many traditional technologies that have been successfully applied for organic wastewater treatment, mainly include physical [1,2], biological [3,4], and chemical methods [5,6], there still has a much big promotion space for the process efficiency and economy. Since 70's of last century, semiconductor photocatalytic technology is booming and considered to be the most prospective method to resolve enhancing environmental and power source problems [7,8]. It can transform sunlight to chemical energy to degrade organic pollutants with environment-friendly and no secondary pollution [9,10]. However, the photogenerated carriers recombination rate of single-component photocatalyst is too fast, which would decrease the light energy utilization and photocatalytic efficiency [11,12]. Therefore, how to enhance the separation of photogenerated carriers is the key to improve the photocatalyst performance.

There are several main strategies for improving the photocatalytic performance of semiconductors: Noble metal deposition [13], ion doping [14], and nanocomposites fabrication [15,16]. In contrast to the former two ways, the preparation of composite semiconductor is to change the transfer path of photogenerated carriers, which would not influence the intrinsic properties of material, and the synthetic method is easy with minimal cost [17,18]. At present, the transfer mode of photoinduced carriers in composite semiconductors are mainly divided into heterojunctions and Z-scheme [19]. Z-scheme simulates the natural photosynthesis mechanism, usually consisting of a reducing end (PS I), an oxidation end (PS II), and an electron transporter (PS I-R-PS II) [20,21]. Compared with the heterojunction, Z-scheme is more conducive to improve the redox capability of the two semiconductors while suppressing the carrier recombination, but it is usually limited by the band position of semiconductor [22]. Therefore, selecting the band matched semiconductors for hybrid has become an important issue for the Z-scheme method.

$BiVO_4$ is a typical ternary metal oxide, which has a narrower band gap, higher response to visible light, and photochemical stability than conventional TiO_2 [23]. The $BiVO_4$ possesses a higher valence band (VB) position, which is appropriate for PS II material [24]. On the other hand, ternary indium-based sulfide AIn_xS_y (A = Cu, Ag, Zn, Cd, and Sn) has been extensively studied in the fields of photocatalysis [25]. Among them, the narrow bandgap of $ZnIn_2S_4$ stands out among many ternary sulfides because of its good response to visible light, green material composition, and

* Corresponding author.
E-mail address: tangshf@ysu.edu.cn (S. Tang).

https://doi.org/10.1016/j.cclet.2019.09.051
1001-8417/

relatively strong photo-corrosion resistance [26], which are suitable as the PS I material. Additionally, the LED light source has low cost and low energy consumption, and its operation is simple and safe, which has attracted much attention recently [27].

Based on above, the coupling of $BiVO_4$ with $ZnIn_2S_4$ would significantly improve charge separation efficiency under visible light irradiation, but the relative report is seldom. Therefore, in this work, a Z-scheme composite was constructed using $ZnIn_2S_4$ as PS I and $BiVO_4$ as PS II to promote the photocatalytic degradation performance under the LED illumination. The Z-scheme composite was fabricated and characterized, and its photodegradation capability was investigated through the methyl orange (MO) decomposition under visible light irradiation, and then the function mechanism was further studied and proposed.

The reagents used in this experiment were introduced in Text S1 (Supporting information). The $BiVO_4$ nanosheets, $ZnIn_2S_4$, and $BiVO_4/ZnIn_2S_4$ (BZ) composite were all prepared by the respective specific hydrothermal methods. Those detailed preparation procedures were described in Text S2 to Text S4 (Supporting information), respectively. Based on the mass ratio of $BiVO_4$ to $ZnIn_2S_4$, the prepared composites were recorded as 1% BZ, 3% BZ, 5% BZ, 10% BZ, and 20% BZ, respectively.

The prepared catalysts were characterized by X-ray diffraction (XRD, D-max-2500), scanning electron microscopy (SEM, SU-PRA55), energy-dispersive X-ray spectroscopy (EDS), X-ray photoelectron spectroscopy (XPS, Thermo Scientific ESCA Lab 250), UV–vis diffuse reflectance spectroscopy spectrophotometer (DRS, UV-3100), nitrogen adsorption (Nova 40000e), Fourier transform infrared spectra spectrometer (FTIR, Necolet IS 10), Raman spectrometer (HORIBA), zeta potential tester (Zetasizer Nano-ZS), and photoluminescence (PL) spectra fluorescence spectrophotometer (Hitachi F-7000). The photoelectric test of this study was tested in the electrochemical workstation CHI660E. The photocatalytic elimination of MO was conducted in a photocatalytic reaction system. All the details of the characterizations and measurements were revealed in Text S5 (Supporting information).

The crystal structure properties for the prepared catalysts were evaluated by XRD. As shown in Fig. 1a, all the diffraction peaks of $BiVO_4$ and $ZnIn_2S_4$ were consistent well with the standard patterns for the pure monoclinic phase of $BiVO_4$ (JCPDS No. 14-0688) and hexagonal phase of $ZnIn_2S_4$ (JCPDS No. 65-2023), respectively [28–30]. The characteristic peak at 28.7° for the 5% BZ proved that the composite was fabricated successfully. Besides, Fig. S1 (Supporting information) displays that most of the diffraction peaks in the composites with different $BiVO_4$ mass ratios were most similar to the diffraction peaks of $ZnIn_2S_4$, which could be due to the decreasing content of $BiVO_4$ in the composite.

To prove the existence and state of each element in $ZnIn_2S_4$, $BiVO_4$, and 5% BZ, the XPS characterization was performed on the three materials (Fig. 1b). It can be seen from the full spectrum that the elements on the surface of these materials had almost the same results as the following EDS analysis (Fig. 2). The C 1s peak was caused by the adsorption of carbonaceous compounds in the atmosphere on the sample surface [31–33]. The other elements in $ZnIn_2S_4$, $BiVO_4$, and 5% BZ were analyzed and discussed in Text S6 and Fig. S2 (Supporting information). Moreover, FTIR and Raman were applied to further characterize and prove the chemical structures of the three materials in Text S7 and Fig. S3 (Supporting information). In addition, the surface pore structure of those materials were determined through nitrogen adsorption-desorption isotherms (Table S1 and Fig. S4 in Supporting information), and the results showed that the combination of $BiVO_4$ and $ZnIn_2S_4$ decreased the surface area of hybrid material, which would affect the adsorption capability of 5% BZ.

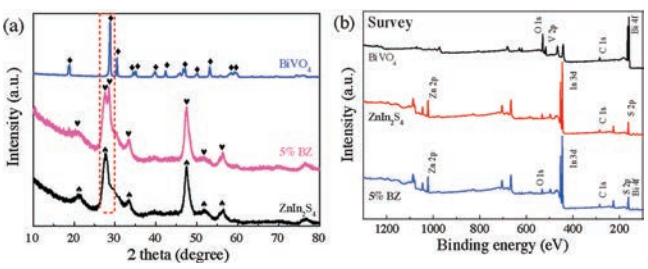

Fig. 1. (a) XRD patterns and (b) XPS spectrum of $BiVO_4$, $ZnIn_2S_4$, and 5% BZ catalysts.

The surface morphologies of the three materials were investigated by SEM. As shown in Fig. 2a, the pure $ZnIn_2S_4$ presented a uniform flower-like microspheres. Fig. 2b shows that the typical sheet-like morphologies were observed on the prepared $BiVO_4$. Fig. 2c displays that the sample of 5% BZ was in the same microsphere shape as $ZnIn_2S_4$. On closer inspection of Fig. 2d, the surface of hybrid material had a more prominent petal-like structure than $ZnIn_2S_4$, which was formed by the intercalation of sheet-like $BiVO_4$ on the microspheres of $ZnIn_2S_4$. The produced intimate combination between $ZnIn_2S_4$ and $BiVO_4$ could be conducive to the electrons transfer from $ZnIn_2S_4$ to $BiVO_4$, so the recombination of photogenerated electron-holes would be suppressed in $ZnIn_2S_4$ [33–35]. The energy dispersive X-ray spectroscopy (EDS) spectrum for the three as-prepared samples indicated that the typical signals of all relevant elements were observed.

The PL spectra of pure $BiVO_4$, $ZnIn_2S_4$, and BZ composites with different $BiVO_4$ content were measured (Fig. 3a). The pure $BiVO_4$ and $ZnIn_2S_4$ presented the stronger PL spectra intensity than the BZ hybrid [36–38]. With the increasing mass percentage of $BiVO_4$, the PL intensity of BZ composites obviously declined, indicating that the photogenerated electron-holes separation degree was augmented after the combination. Besides, as seen in Fig. 3b for the photocurrent measurement, 5% BZ displayed an obvious improved photocurrent, which produced a photocurrent of 1.4 $\mu A/cm^2$, while the photocurrents were only 1.0 $\mu A/cm^2$ and 0.7 $\mu A/cm^2$ for $BiVO_4$ and $ZnIn_2S_4$, respectively. Fig. 3c shows that the order of electrochemical impedance curvature of three curves from large to small was $BiVO_4$ > $ZnIn_2S_4$ > 5% BZ, demonstrating that the photogenerated electron-holes separation of 5% BZ was the highest [39,40]. Above results can be concluded that the combination of $BiVO_4$ and $ZnIn_2S_4$ represented a synergistic effect, inhibiting the photo-generated electron-holes recombination and promoting the efficient separation of photogenerated carriers, and thus can improve the photocatalytic performance. Furthermore, the UV–vis DRS spectra testified that 5% BZ had a wider response range to visible light than the pure $BiVO_4$ and $ZnIn_2S_4$ (Fig. S5 in Supporting information).

The photocatalytic degradations of $BiVO_4$, $ZnIn_2S_4$, and BZ composites with different $BiVO_4$ mass ratio were investigated for the decolorization of MO (Fig. 3d). The experimental conditions were as follows: MO concentration 15 mg/L, initial pH 6.3, and catalyst dosage 0.20 g/L. Before the photocatalytic test begins, a 30 min dark reaction process was conducted to reach absorption equilibrium. The adsorption performances of the composites were slightly lower than that of pure $ZnIn_2S_4$. This is because that the specific surface area and pore volume of the hybrids both decreased after combination. After 240 min photocatalytic reaction, pure $BiVO_4$ presented the lowest photocatalytic efficiency of 17% (corresponding rate constant 0.000963 min^{-1}), meanwhile $ZnIn_2S_4$ achieved a decolorization of 62% (0.00515 min^{-1}). For the series of BZ composites, the decolorization rate displayed an increase and decrease trend with the enhancing mass percentage of $BiVO_4$ from 1% to 20%. Therein, 5% BZ reached the highest decolorization rate of 86% (0.00997 min^{-1}), which was 1.9 and 10.3

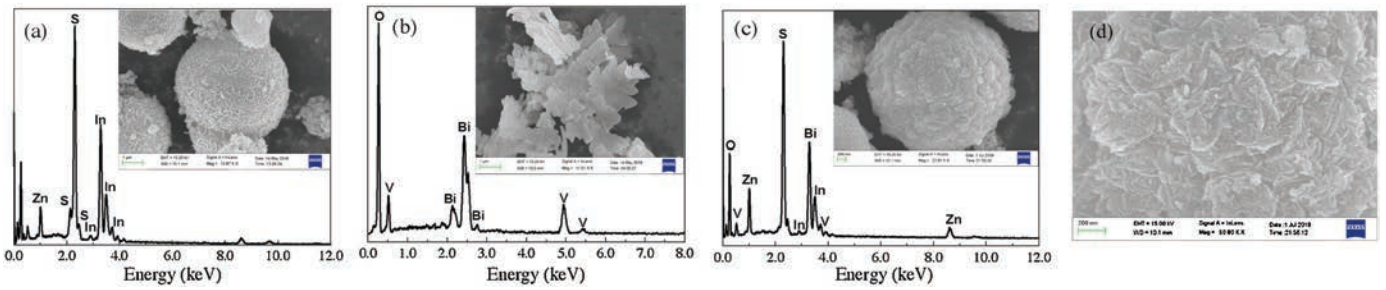

Fig. 2. SEM images and EDS of (a) $ZnIn_2S_4$, (b) $BiVO_4$, and (c, d) 5% BZ.

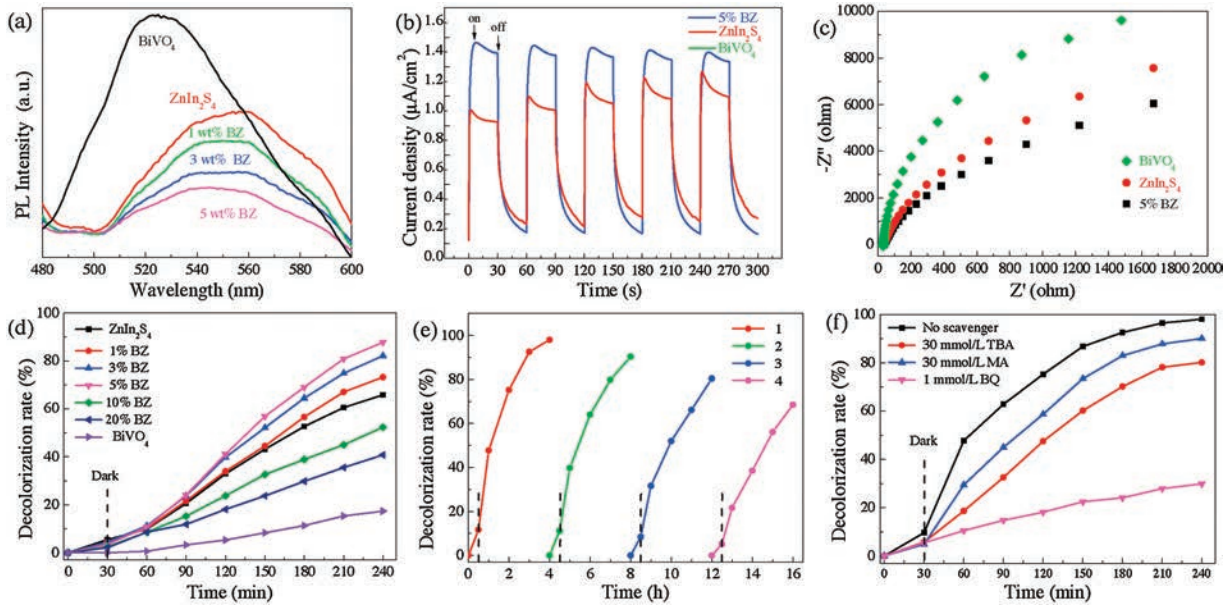

Fig. 3. PL spectra (a), transient photocurrent density (b), and electrochemical impedance spectroscopy (c) of $BiVO_4$ $ZnIn_2S_4$, and different BZ. (d) Time courses of MO decolorization for $BiVO_4$, $ZnIn_2S_4$, and $BiVO_4/ZnIn_2S_4$ with different $BiVO_4$ content under visible light irradiation. (e) Consecutive adsorption and photocatalytic tests of 5% BZ for MO decolorization. (f) Free radicals scavenging test for 5% BZ.

times higher than pure $ZnIn_2S_4$ and $BiVO_4$, respectively. But when the $BiVO_4$ loading amount exceeded 5%, the decolorization efficiency gradually decreased, only 52% (0.00402 min^{-1}) and 40% (0.00213 min^{-1}) for 10% BZ and 20% BZ, respectively, which were even lower than that of $ZnIn_2S_4$. The optimal photocatalytic performance of 5% BZ could be ascribed to its better separation for photogenerated electron-holes. Besides, the photostability of 5% BZ was investigated by the consecutive adsorption and photocatalytic decomposition of MO (Fig. 3e). After four times repeated applications, the composite presented the analogical removal trend and rate, which could be ascribed to the well separation of photogenerated carriers for 5% BZ, proving it possessed a certain photostability.

The further degradation and mineralization of MO by 5% BZ in the photocatalytic process were assessed through the UV–vis spectra, chemical oxygen demand (COD) and total organic carbon (TOC) analyses (Figs. S6 and S7 in Supporting information). The COD and TOC removing efficiencies of 5% BZ were both higher than those of $ZnIn_2S_4$, indicating the better degradation and mineralization effects on the MO for 5% BZ.

A certain amount of methanol (MA), *tert*-butanol (TBA), and *p*-benzoquinone (BQ) were introduced as inhibitors of h^+, $^{\bullet}OH$, and $^{\bullet}O_2^-$ to investigate the photo-degradation mechanism, respectively (Fig. 3f) [41–43]. After 4 h irradiation, the decolorization ratios for

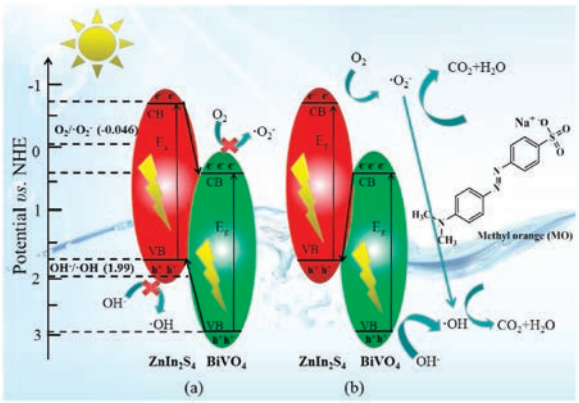

Fig. 4. Photocatalysis mechanism for $BiVO_4/ZnIn_2S_4$ composite. (a) Heterojunctions path; (b) Z-scheme path.

the adding 30 mmol/L of MA and TBA were 86% and 78%, respectively. However, only 1 mmol/L BQ declined the MO removal to 29%. During the photocatalytic process, the photogenerated e^- could react with O_2 to form $^{\bullet}O_2^-$ and $^{\bullet}OH$ would be produced

through h^+ oxidative process on H_2O or OH^-. Besides, not only $^{\bullet}O_2^-$ plays a key role in the organics photodegradation, but also participate in the $^{\bullet}OH$ generation in the reactive species chain reactions [44–47].

Based on above results and discussions, the assumption for the BZ composite was depicted in Fig. 4. According to heterojunctions function as in the Fig. 4a, there would be hard to generate $^{\bullet}O_2^-$ and $^{\bullet}OH$ [48,49]. Nevertheless, previous results testified the existence of $^{\bullet}O_2^-$ and $^{\bullet}OH$, so the heterojunctions assumption is untenable. As seen in the Z-scheme path (Fig. 4b), e^- on conduction band (CB) of $BiVO_4$ would migrate to the VB of $Znln_2S_4$ under illumination. Especially, e^- produced by $BiVO_4$ would be recombined with h^+ form by $ZnIn_2S_4$, which could inhibit the recombination of e^- and h^+ for $Znln_2S_4$ and $BiVO_4$, respectively. Hence, for Z-scheme composite, e^- and h^+ would be aggregated on the CB of $ZnIn_2S_4$ and the VB of $BiVO_4$, respectively [50]. The CB position of $ZnIn_2S_4$ is −0.68 eV, which is much lower than the $O_2/^{\bullet}O_2^-$ redox (−0.33 eV), so it is more favorable for the reaction with O_2 adsorbed on the composite surface to produce $^{\bullet}O_2^-$. Meanwhile, the VB position of $BiVO_4$ is at +2.98 eV, which is much higher than that of $OH^-/^{\bullet}OH$ (+2.4 eV), which is beneficial to $^{\bullet}OH$ production. In addition, h^+ on $BiVO_4$ can also directly participate in the reaction. Above Z-scheme path was proved by previous characterizations and photocatalytic tests.

To sum up, the $BiVO_4/ZnIn_2S_4$ all-solid-state Z-scheme composite with the excellent photocatalytic performance under the LED visible light illumination was constructed. The highest MO decolorization rate of 86% (corresponding rate constant 0.00997 min^{-1}), was achieved over 5% BZ nanocomposite, which was higher than pure $BiVO_4$ and $ZnIn_2S_4$. The Z-scheme composite demonstrated good photocatalytic degradation of MO because its enhanced separation for photogenerated electron-holes, thus promoting the photocatalytic performance and reactive species generation. This work proved that constructing an all-solid-state Z-scheme nanocomposite is a hopeful method to improve the photocatalytic degradation for organic wastewater of photocatalyst.

Declaration of competing interests

The authors declare that they have no known competing financial interests or personal relationships that could have appeared to influence the work reported in this paper.

Acknowledgements

We are thankful to the financial supports from the National Natural Science Foundation of China (Nos. 51908485 and 51608468), the China Postdoctoral Science Foundation (No. 2019T120194), the University Science and Technology Program Project of Hebei Provincial Department of Education (No. QN2018258).

Appendix A. Supplementary data

Supplementary material related to this article can be found, in the online version, at doi:https://doi.org/10.1016/j.cclet.2019.09.051.

References

[1] Q. Zhang, S. Bolisetty, Y. Cao, et al., Angew. Chem. Int. Ed. 58 (2019) 6012–6016.
[2] Q. Zhang, Y. Han, L. Wu, Chem. Eng. J. 363 (2019) 278–284.
[3] C. Grandclément, I. Seyssiecq, A. Piram, et al., Water Res. 111 (2017) 297–317.
[4] J. Li, B. Li, H. Huang, et al., Sci. Total Environ. 687 (2019) 460–469.
[5] K. Ma, W. Chen, T. Jiao, et al., Chem. Sci. 10 (2019) 6821–6827.
[6] S. Yang, K. Yin, J. Wu, et al., Nanoscale 11 (2019) 17607–17614.
[7] A. Fujishima, K. Honda, Nature 238 (1972) 37–38.
[8] Y. Hou, M. Qiu, M.G. Kim, et al., Nat. Commun. 10 (2019) 1392.
[9] M. Gmurek, M. Olak-Kucharczyk, S. Ledakowicz, Chem. Eng. J. 310 (2017) 437–456.
[10] G. Xia, C. Li, K. Wang, L. Li, Sci. Adv. Mater. 11 (2019) 1079–1086.
[11] J. Liu, J. Zhang, D. Wang, et al., ACS Sustain. Chem. Eng. 7 (2019) 12428–12438.
[12] J. Ke, M. Adnan Younis, Y. Kong, et al., Nano-Micro Lett. 10 (2018).
[13] Y. Chen, Y. Wang, W. Li, et al., Appl. Catal. B.-Environ. 210 (2017) 352–367.
[14] B. Huang, J. He, S. Bian, et al., Chin. Chem. Lett. 29 (2018) 1698–1701.
[15] J. Ke, J. Liu, H. Sun, et al., Appl. Catal. B.-Environ. 200 (2017) 47–55.
[16] M. Ji, Z. Zhang, S. Zhang, et al., Chin. Chem. Lett. 29 (2018) 805–810.
[17] Y. Hong, Y. Jiang, C. Li, et al., Appl. Catal. B.-Environ. 180 (2016) 663–673.
[18] Y. Zhang, D. Zhang, X. Xu, B. Zhang, Chin. Chem. Lett. 29 (2018) 1350–1354.
[19] J. Chen, J. Zhan, Y. Zhang, Y. Tang, Chin. Chem. Lett. 30 (2019) 735–738.
[20] P. Zhou, J. Yu, M. Jaroniec, Adv. Mater. 26 (2014) 4920–4935.
[21] H. Zhou, Z. Wen, J. Liu, et al., Appl. Catal. B.-Environ. 242 (2019) 76–84.
[22] L. Ye, J. Liu, C. Gong, et al., ACS Catal. 2 (2012) 1677–1683.
[23] F. Chen, Q. Yang, Y. Wang, et al., Chem. Eng. J. 348 (2018) 157–170.
[24] F. Ye, H. Li, H. Yu, S. Chen, X. Quan, Appl. Catal. B.-Environ. 227 (2018) 258–265.
[25] Z. Guan, Z. Xu, Q. Li, et al., Appl. Catal. B.-Environ. 227 (2018) 512–518.
[26] S. Wan, M. Ou, Q. Zhong, S. Zhang, F. Song, Chem. Eng. J. 325 (2017) 690–699.
[27] Y. Gao, S. Li, Y. Li, L. Yao, H. Zhang, Appl. Catal. B.-Environ. 202 (2017) 165–174.
[28] M. Ou, S. Wan, Q. Zhong, et al., Appl. Catal. B.-Environ. 221 (2018) 97–107.
[29] C. Duan, F. Li, M. Yang, et al., Ind. Eng. Chem. Res. 57 (2018) 15385–15394.
[30] C. Duan, Y. Cao, L. Hu, et al., J. Hazard. Mater. 373 (2019) 141–151.
[31] M. Zhu, Z. Sun, M. Fujitsuka, T. Majima, Angew. Chem. Int. Ed. 130 (2018) 2182–2186.
[32] H. Guo, N. Jiang, H. Wang, et al., Appl. Catal. B.-Environ. 248 (2019) 552–566.
[33] K. Wang, L. Li, Y. Lan, P. Dong, G. Xia, Math. Probl. Eng. 2019 (2019) 1–8.
[34] N. Jiang, C. Qiu, L. Guo, et al., J. Hazard. Mater. 369 (2019) 611–620.
[35] F. Chen, H. Huang, Y. Zhang, T. Zhang, Chin. Chem. Lett. 28 (2017) 2244–2250.
[36] X. Zhang, J. Xiao, M. Hou, Y. Xiang, H. Chen, Appl. Catal. B.-Environ. 224 (2018) 871–876.
[37] P. Huo, J. Li, Z. Ye, et al., Chin. Chem. Lett. 28 (2017) 2259–2262.
[38] Y. Zhou, Y. Huang, J. Pang, K. Wang, J. Power Sources 440 (2019) 227149.
[39] Z. Luo, L. Qu, J. Jia, et al., Chin. Chem. Lett. 29 (2018) 547–550.
[40] H. Li, S. Guo, K. Shin, M.S. Wong, G. Henkelman, ACS Catal. 9 (2019) 7957–7966.
[41] N. Jiang, Y. Zhao, C. Qiu, et al., Appl. Catal. B.-Environ. 259 (2019) 118061.
[42] T. Zhang, X. Li, Q. Zhao, Y. Rao, Sustain. Cities Soc. 51 (2019) 101714.
[43] X. Nie, S. Feng, Z. Shudu, G. Quan, Adv. Civ. Eng. Mater. 2019 (2019) 1–12.
[44] S. Tang, N. Li, D. Yuan, et al., Chemosphere 234 (2019) 658–667.
[45] D. Yuan, C. Zhang, S. Tang, et al., Water Res. (2019) 114861.
[46] Y. He, X. Zhuang, C. Lei, et al., Nano Today 24 (2019) 103–119.
[47] H. Huang, S. Tu, C. Zeng, et al., Angew. Chem. Int. Ed. 56 (2017) 11860–11864.
[48] K. Wu, H. Yang, L. Jia, et al., Green Chem. 21 (2019) 1472–1483.
[49] D. Liu, Y. Cao, J. Liu, Y. Gao, Y. Wang, J. Eur. Ceram. Soc. 38 (2018) 817–820.
[50] Y. He, R. Wang, T. Jiao, et al., ACS Sustain. Chem. Eng. 7 (2019) 10888–10899.